Brazilian Journal of Geophysics, 41 (2023), 1, 1–22
Brazilian Geophysical Society
ISSN 2764-8044
DOI: 10.22564/brjg.v41i1.2203

BARBIERI CRITERION FOR SOLUTION APPRAISAL IN GEOPHYSICAL DIFFRACTION TOMOGRAPHY

Daniel Walter da Silva Mascarenhas [1] and Amin Bassrei [2] *

[1] Universidade Federal da Bahia - UFBA, Institute of Geosciences, Salvador, BA, Brazil
[2] Universidade Federal da Bahia - UFBA, Research Center in Geophysics and Geology, Institute of Geosciences and National Institute of Science and Technology in Petroleum Geophysics, Salvador, BA, Brazil

*Corresponding author email: bassrei@gmail.com

ABSTRACT. Diffraction tomography provides a high resolution velocity image from the region under study. Because it is a type of ill-conditioned inverse problem, diffraction tomography requires some kind of regularization, such as regularization by derivative matrices. Quantitative or qualitative criteria for the solution appraisal of inverse problems are just as important as the solution itself. An effective criterion is the Barbieri approach, which is the main scope in this study. It is implemented in three steps: (i) the estimated model obtained through the inversion of the observed data (scattered acoustic field); (ii) a second inversion, this time of the complementary observed data which provides the complementary estimated model; (iii) the sum of the estimated model and complementary estimated model. If the inversion is exact, this sum must be a constant value for the whole vector. If this does not occur, the sum image indicates that the inversion was not satisfactory (quantitative effect) and in which regions the estimated model was not well recovered (qualitative effect). Simulations were performed on two synthetic models, one with well-to-well geometry and the other with surface seismics geometry. The results, confronted with the RMS deviation between the estimated and the true model, validated the use of the Barbieri criterion in diffraction tomography.

Keywords: inverse problems; diffraction tomography; solution appraisal; Barbieri criterion....

Introduction

Diffraction tomography is an inversion technique that allows the estimation of the velocity distribution in the subsurface. Furthermore, this technique has applications in imaging problems in several fields, such as medicine and geophysics. The input data are the amplitudes of seismic signals recorded in the receivers. The pioneering works applying diffraction tomography in geophysics were done published by Devaney (1984), Harris (1987) and Wu & Toksöz (1987). These authors used the filtered retropropagation approach, while a matrix approach was used by Lo & Inderwiesen (1994). The advantages of the use of multiple frequencies have been presented by several authors, like for instance, Sande et al. (2019).

The medium of interest is usually parameterized in small cells or blocks, where the physical property is constant in each block. Diffraction tomography estimates the object function, which is proportional to the velocity of each block. For a given array of acoustic sources distributed along a well and/or on the surface, the input data is the scattered field measured at the receivers located in a second well and/or on the surface.

Diffraction tomography is an ill-posed inverse problem, which requires some regularization technique. The question of the regularization of the inverse problem and the search for the optimal normalization parameter λ was studied by Santos & Bassrei (2007), who used the L curve and the Theta curve to choose λ. More recently, Santos et al. (2021) used generalized cross validation for the same purpose.

Because it is a high resolution method, diffraction tomography is used in reservoir geophysics. It has also been used to monitor CO_2 injection (Santos et al., 2009; Silva & Bassrei, 2016).

One important issue in inverse problems is the validation of the estimated solution. In fact, a quantitative criterion for the solution appraisal is just as important as the solution itself. In simulations with synthetic data, the estimated model can be quantitatively compared with the true model, through the RMS deviation between the two models. However, the true model is never available on real data.

An effective criterion is the Barbieri (1974) approach, which is the main scope in this study. It was originally developed as an evaluation criterion in medical imaging. Barbieri (1974) defined a reference matrix $\mathbf{W}$, composed of constant elements. Then, the estimated model is obtained through the inversion of the observed data. A second inversion, this time of the complementary observed data which provides the complementary estimated model. The sum of the estimated model and complementary estimated model is stored as a matrix, denoted by $\mathbf{W}^{est}$. If the inversion is exact, $\mathbf{W}^{est}$ must be a constant value for the whole matrix, that is, the closer the matrix $\mathbf{W}^{est}$ is to the reference matrix $\mathbf{W}$, the better the quality of the inversion.

Bejarano & Bassrei (2017) showed that the Barbieri criterion can be used qualitatively and quantitatively, in an application in traveltime tomography. From a qualitative point of view, the image given by the matrix allows identifying any regions in the subsurface where the inversion was not satisfactory. And, from a quantitative point of view, it is possible to calculate an RMS estimator of deviations between the matrices $\mathbf{W}$ and $\mathbf{W}^{est}$.

We use the solution appraisal approach in two synthetic models, each with a specific data acquisition geometry, either well-to-well seismics or surface seismics. With the Barbieri's criterion, the proximity between the two matrices confirmed that the estimated model was satisfactory in the results of the first synthetic data. As for the second synthetic model, the two matrices are visually a little different. In this case, it can then be verified in which spatial portions of the estimated model, the inversion was not satisfactory. In the two synthetic models, the RMS deviation between $\mathbf{W}^{est}$ and $\mathbf{W}$ was quantitatively evaluated, which allowed to compare different results of the same synthetic model.

Review of Inverse Problems

The inverse method uses data as input and aims to arrive at an estimated model, represented by model parameters. Even in cases where a solution exists, such a solution is usually not unique. And if uniqueness is guaranteed, the question of stability may still be present. Thus, inverse problems in geophysics are generally ill-posed. Therefore, it is necessary to use some resource to circumvent this issue (Menke, 2018).

The linear relationship between the model parameter vector $\mathbf{m}$ and the observed data vector $\mathbf{d}$ is expressed as:

$$\mathbf{d} = \mathbf{G}\mathbf{m}. \tag{1}$$

The operator $\mathbf{G}$ has M rows and N columns, so that the generalized inverse operator $\mathbf{G}^{+}_{NXM}$ (Penrose, 1955), with N rows and M columns, can be obtained through the decomposition by singular values. The regularization by derivative matrices, proposed by Twomey (1963), considers a linear operator $\mathbf{D_n}$, with n being the order of the operator, and an auxiliary vector $\mathbf{l_n}$, in such a way that,

$$\mathbf{l_n} = \mathbf{D_n}\mathbf{m}. \tag{2}$$

Thus, a scalar operator L_n is expressed as:

$$L_n = \|\mathbf{l_n}\|_2^2 = (\mathbf{D_n m})^T (\mathbf{D_n m}). \tag{3}$$

For the case of a second order operator, the vector $\mathbf{l_n}$ is given by:

$$\mathbf{l}_2 = \begin{pmatrix} 1 & -2 & 1 & 0 & \cdots & 0 & 0 & 0 & 0 \\ 0 & 1 & -2 & 1 & \cdots & 0 & 0 & 0 & 0 \\ \vdots & \vdots & \vdots & \vdots & \ddots & \vdots & \vdots & \vdots & \vdots \\ 0 & 0 & 0 & 0 & \cdots & 0 & 1 & -2 & 1 \end{pmatrix} \begin{pmatrix} m_1 \\ m_2 \\ \vdots \\ m_N \end{pmatrix} = \mathbf{D}_2\mathbf{m}. \tag{4}$$

The objective function that we use is expressed as:

$$\Phi(\mathbf{m}) = \mathbf{e}^{\mathbf{T}}\mathbf{e} + \lambda[(\mathbf{D}_2\mathbf{m})^T (\mathbf{D}_2\mathbf{m})], \tag{5}$$

where $\mathbf{e} = \mathbf{d}^{obs} - \mathbf{G}\mathbf{m}$.

Notice that besides the least squares method, a constraint representing the regularization process was used. Minimizing equation (5) in relation to the model parameters, we obtain:

$$\mathbf{m} = \mathbf{m}^{\mathbf{est}} = (\mathbf{G}^{\mathbf{T}}\mathbf{G} + \lambda\mathbf{D}_2^{\mathbf{T}}\mathbf{D}_2)^{-1}\mathbf{G}^{\mathbf{T}}\mathbf{d}. \tag{6}$$

Barbieri's Criterion

In the approach suggested by Barbieri (1974), we consider an auxiliary vector, called complementary model, whose sum with the true model results in a constant vector, expressed by $\mathbf{w}$:

$$\mathbf{m}^{true} + \mathbf{m}^{true,c} = \mathbf{w}.$$

(7)

Multiplying equation (7) by the matrix $\mathbf{G}$ on the left, we have:

$$\mathbf{G}\mathbf{m}^{true} + \mathbf{G}\mathbf{m}^{true,c} = \mathbf{G}\mathbf{w}.$$

(8)

As $\mathbf{G}\mathbf{m}^{true} = \mathbf{d}^{obs}$ and also defining $\mathbf{G}\mathbf{m}^{true,c} = \mathbf{d}^{obs,c}$, where $\mathbf{d}^{obs,c}$ is called complementary observed data, equation (8) can be written as:

$$\mathbf{d}^{obs,c} = \mathbf{G}\mathbf{w} - \mathbf{d}^{obs}.$$

(9)

Using the same formalism to determine the estimated solution, the complementary estimated solution $\mathbf{m}^{est,c}$ can be obtained from the given complementary vector $\mathbf{d}^{obs,c}$:

$$\mathbf{m}^{est,c} = \left(\mathbf{G}^{\mathrm{T}}\mathbf{G} + \lambda \mathbf{D}_2^{\mathrm{T}}\mathbf{D}_2\right)^{-1}\mathbf{G}^{\mathrm{T}}\mathbf{d}^{obs,c}.$$

(10)

Finally, from the estimated model $\mathbf{m}^{est}$ and the complementary estimated model $\mathbf{m}^{est,c}$ we obtain the vector $\mathbf{w}^{est}$:

$$\mathbf{w}^{est} = \mathbf{m}^{est} + \mathbf{m}^{est,c}.$$

(11)

For a linear, exact, and stable inverse problem, this sum must result into a constant value. The one-dimensional vector $\mathbf{w}^{est}$ can be graphically represented as a matrix, denoted by $\mathbf{W}^{est}$, in the same way that the model parameters vector, whether true or estimated, can be presented visually in two dimensions. The estimated model can be inspected visually, that is, a qualitative interpretation can be carried out in order to verify in which portions of the image the inversion was unsatisfactory (Bassrei, 2000).

The result of the inversion can be quantitatively evaluated by estimating the square root of the mean square value (RMS), in this case considering the relative percentage deviation (Bejarano & Bassrei, 2017):

$$\varepsilon_w = \frac{\sqrt{\sum_{i=1}^{N}(w_i - w_i^{est})^2}}{\sqrt{\sum_{i=1}^{N}(w_i)^2}} \times 100\%.$$

(12)

Diffraction Tomography

The wave equation for an infinite acoustic medium is given as:

$$\nabla^2\Psi(\mathbf{r},t) = \frac{1}{c^2(\mathbf{r})}\frac{\partial^2\Psi(\mathbf{r},t)}{\partial t^2},$$

(13)

where $\Psi(\mathbf{r},t)$ is the acoustic wavefield, $\mathbf{r}$ is the position vector, $c(\mathbf{r})$ is the velocity as a function of position and ∇^2 is the Laplacian operator. The solution to be determined can be decomposed as (Lo & Inderwiesen, 1994):

$$\Psi(\mathbf{r},t) = e^{-i\omega t}P(\mathbf{r},t).$$

(14)

Calculating the Fourier transform of equation (14), and substituting into equation

(13), we obtain the Helmholtz equation:

$$\nabla^2 P(\mathbf{r},\omega) + \kappa^2(\mathbf{r},\omega)P(\mathbf{r},\omega) = 0,$$

(15)

where ω is the angular frequency and $\kappa(\mathbf{r},\omega)$ is the wave number, given by:

$$\kappa(\mathbf{r},\omega) = \frac{\omega}{c(\mathbf{r})}. \quad (16)$$

The wavefield recorded in the receiver is called the total field, as it has a contribution from the incident field and also from the scattered field, that is, $P_T(\mathbf{r}) = P_I(\mathbf{r}) + P_S(\mathbf{r})$, where the index I indicates incident and S scattered. With this, the Helmholtz equation is expressed as:

$$[\nabla^2 + \kappa^2(\mathbf{r})][P_I(\mathbf{r}) + P_S(\mathbf{r})] = 0. \quad (17)$$

We define the object function $M(\mathbf{r})$ as:

$$M(\mathbf{r}) = \left[1 - \frac{c_0^2}{c^2(\mathbf{r})}\right],$$

(18)

so that if the velocity in the inhomogeneous medium is equal to the constant value, the object function vanishes. Replacing equation (18) into equation (17):

$$[\nabla^2 + \kappa_0^2]P_S(\mathbf{r}) = \kappa_0^2 M(\mathbf{r})[P_I(\mathbf{r}) + P_S(\mathbf{r})].$$

(19)

Equation (19) has an integral solution, known as the Lippmann-Schwinger equation, and expressed as:

$$P_S(\mathbf{r}) = -\kappa_0^2 \int_A G(\mathbf{r}\,|\,\mathbf{r}')M(\mathbf{r})[P_I(\mathbf{r}) + P_S(\mathbf{r})]d\mathbf{r}',$$

(20)

where $\mathbf{r}$ is the observer position, $\mathbf{r}'$ is the source position and $G(\mathbf{r}\,|\,\mathbf{r}')$ is the Green's function, given by:

$$G(\mathbf{r}\,|\,\mathbf{r}') = \frac{i}{4} H_0^{(1)}\left(\kappa_0\,|\,\mathbf{r} - \mathbf{r}'|\right),$$

(21)

being $H_0^{(1)}$ the Hankel function of the first type and order zero.

We will use the first-order Born approximation,

$$P_S(\mathbf{r}) << P_I(\mathbf{r}),$$

(22)

so that

$$P_S(\mathbf{r}) + P_I(\mathbf{r}) \approx P_I(\mathbf{r}),$$

(23)

and the Lippmann-Schwinger equation is approximated as:

$$P_S(\mathbf{r}) \approx -\kappa_0^2 \int_A G(\mathbf{r}\,|\,\mathbf{r}') M(\mathbf{r}) P_I(\mathbf{r}) d\mathbf{r}'.$$

(24)

Considering that the source is a pulse located at $\mathbf{r}_s$, $P_I(\mathbf{r})$ can be expressed by:

$$P_I(\mathbf{r}) = G(\mathbf{r}\,|\,\mathbf{r}_s).$$

(25)

Substituting equation (25) into equation (24) we have:

$$P_S(\mathbf{r}_s, \mathbf{r}_r) \approx -\kappa_0^2 \int_A M(\mathbf{r}) G(\mathbf{r}'|\,\mathbf{r}_s) G(\mathbf{r}_r\,|\,\mathbf{r}') d\mathbf{r}'. \quad (26)$$

Numerical Simulations

Model A, shown in Figure 1(a), is composed of a series of layers forming an anticline. This model has 800 square blocks, each block having an edge of 10 m. Therefore, there are 800 parameters to be estimated in the reverse procedure.

Three configurations with the well-to-well geometry were considered: (i) underdetermined case with 10 sources and 20 receivers, which implies 200 source-receiver pairs; (ii) determined case with 20 sources and 20 receivers, which now implies 400 source-receiver pairs; (iii) finally, the overdetermined case with 40 sources and 20 receivers, that is, 800 source-receiver pairs. As the scattered field is a complex variable, the observed data vector, which is the input of the inversion, is composed of the real values of the field, followed by the imaginary values. This doubles the number of elements in the observed data vector, as well as doubles the number of rows in the tomographic matrix. For example, for the determined case, the 400 source-receiver pairs result in 800 equations, which confirms the dimensions of this, determined, configuration.

Matrix $\mathbf{W}$ is shown in Figure 1(b), where it can be seen that all elements are equal. For this model, the constant value of 0.3 was adopted. This value is dimensionless since the object function is also dimensionless.

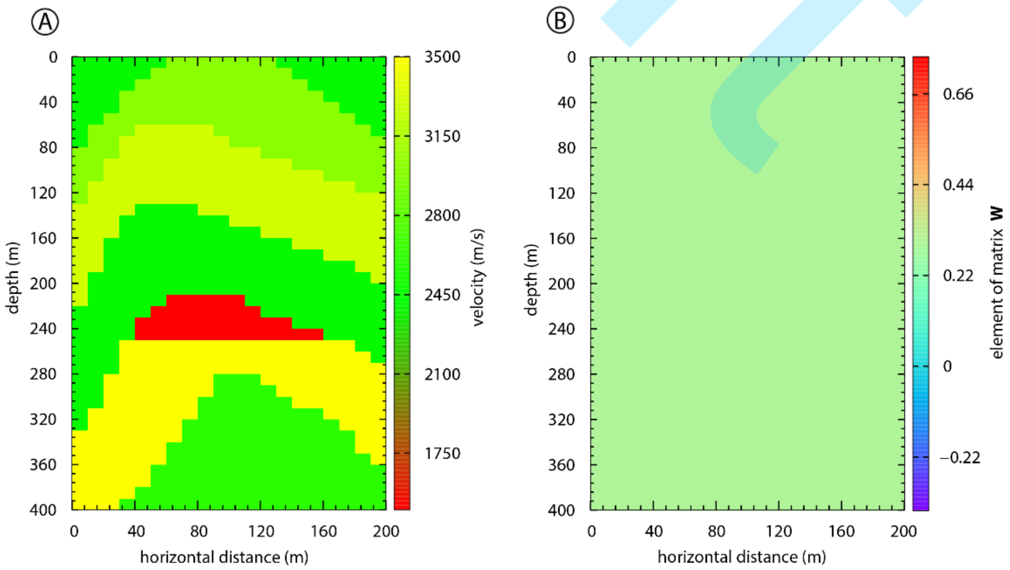

Figure 1: Model A. (a) True model with 800 blocks, where the color bar indicates the propagation P-wave velocity. The low velocity geological feature in red represents an oil reservoir. (b) True matrix $\mathbf{W}$ with a constant value w_{ij} = 0.30 (dimensionless).

The generalized inverse approach (Penrose, 1955) was used, through singular value decomposition. To deal with the ill-posed aspect of the inverse problem, regularization by derivatives matrices was used. The regularization procedure demands the choice of a regularization factor, denoted by λ. The selection of λ is a problem by itself. Santos & Bassrei (2007) addressed the selection of the regularization factor using the L-curve and comparing it to the proposed Θ-curve. Silva & Bassrei (2016) applied generalized cross validation (GCV) in diffraction tomography for CO_2 monitoring. Santos et al. (2021) applied GCV in diffraction tomography comparing different data acquisition geometries. However, in this work the regularization factor was chosen by trial and error. In all simulations of this model, the working frequency of 50 Hz was adopted.

To validate the inversion technique, the observed data vector (scattered field) was corrupted with random noise. For quantitative purposes, the deviation between the observed data $\mathbf{d}^{obs}$ and the observed data corrupted with noise $\mathbf{d}^{obs,*}$ is calculated by the RMS estimator:

$$\varepsilon_{noise} = \sqrt{\frac{\sum_{i=1}^{M}(d_i^{obs} - d_i^{obs,*})^2}{\sum_{i=1}^{M}(d_i^{obs})^2}} \times 100\%, \qquad (27)$$

Two noise levels were considered: $\varepsilon_{noise} = 1\%$, $\varepsilon_{noise} = 5\%$, in addition to the case without noise, $\varepsilon_{noise} = 0$.

Table 1 shows the results of nine simulations. For each data configuration – underdetermined, determined and overdetermined, as above mentioned, three levels of noise were tested: (i) without added noise, (ii) noise with 1% RMS deviation and (iii) noise with 5% RMS deviation. For each simulation we present the errors of the model parameters (object function), the data (scattered field) and the vector $\mathbf{w}$ using, respectively, the following relative RMS estimators:

$$\varepsilon_m = \sqrt{\frac{\sum_{i=1}^{N}(m_i^{true}-m_i^{est})^2}{\sum_{i=1}^{N}(m_i^{true})^2}} \times 100\%, \tag{28}$$

$$\varepsilon_d = \sqrt{\frac{\sum_{i=1}^{M}(d_i^{obs}-d_i^{cal})^2}{\sum_{i=1}^{M}(d_i^{obs})^2}} \times 100\%, \tag{29}$$

and

$$\varepsilon_w = \sqrt{\frac{\sum_{i=1}^{N}(w_i-w_i^{est})^2}{\sum_{i=1}^{N}(w_i)^2}} \times 100\%. \tag{30}$$

Due to space limitations, we present only three results for model A in figure form. Figure 2 shows the inversion for the determined case, with noise-free data. Figure 2(a) shows the estimated model and Figure 2(b) the complementary estimated model. The sum of these two images is shown in Figure 2(c), where we can see the image is virtually constant, that is, the matrix $\mathbf{W}^{est}$ is equal to the matrix $\mathbf{W}$, shown in Figure 1(b). Therefore, Figure 2(c) confirms the quality of the result shown in Figure 2(a). The P-wave velocity is shown in Figure 2(d), which shows a fluctuation if compared to Figure 2(a). This is due to the scale effect, that is, a small variation in the object function is equivalent to a considerable variation in the absolute value of the velocity.

Table 1: Inversion results of model A. The first three rows refer to the underdetermined case, the next three rows refer to the determinate case, and the last three rows present the results for the overdetermined case. The first column indicates the noise level. The second, third and fourth columns show the RMS deviations, respectively, between $\mathbf{d}^{obs}$ and $\mathbf{d}^{pre}$, $\mathbf{m}^{true}$ and $\mathbf{m}^{est}$, $\mathbf{w}$ and $\mathbf{w}^{est}$.

Noise (%)	ε_d (%)	ε_m (%)	ε_w (%)
0	≈ 0	69.42	≈ 0

1	≈ 0	72.90	≈ 0
5	≈ 0	98.34	226.45
0	≈ 0	2.04	0.43
1	1.23	9.81	6.97
5	2.73	12.18	23.39
0	≈ 0	≈ 0	≈ 0
1	6.84	6.60	3.87
5	15.17	10.79	21.01

The value of 0.3 is selected in such a way that the equation (7) is satisfied. Notice that equation (7) is still valid for the estimated values, instead of the true values, if the inversion is exact. In Figure 2(a), $\mathbf{m}^{est}$ varies roughly from -2.0 to 0.5 and in Figure 2(b) $\mathbf{m}^{est,c}$ varies roughly from -0.5 to 2.0. At any point of the estimated model, the sum of $\mathbf{m}^{est}$ and $\mathbf{m}^{est,c}$ is 0.3, making it an appropriate value.

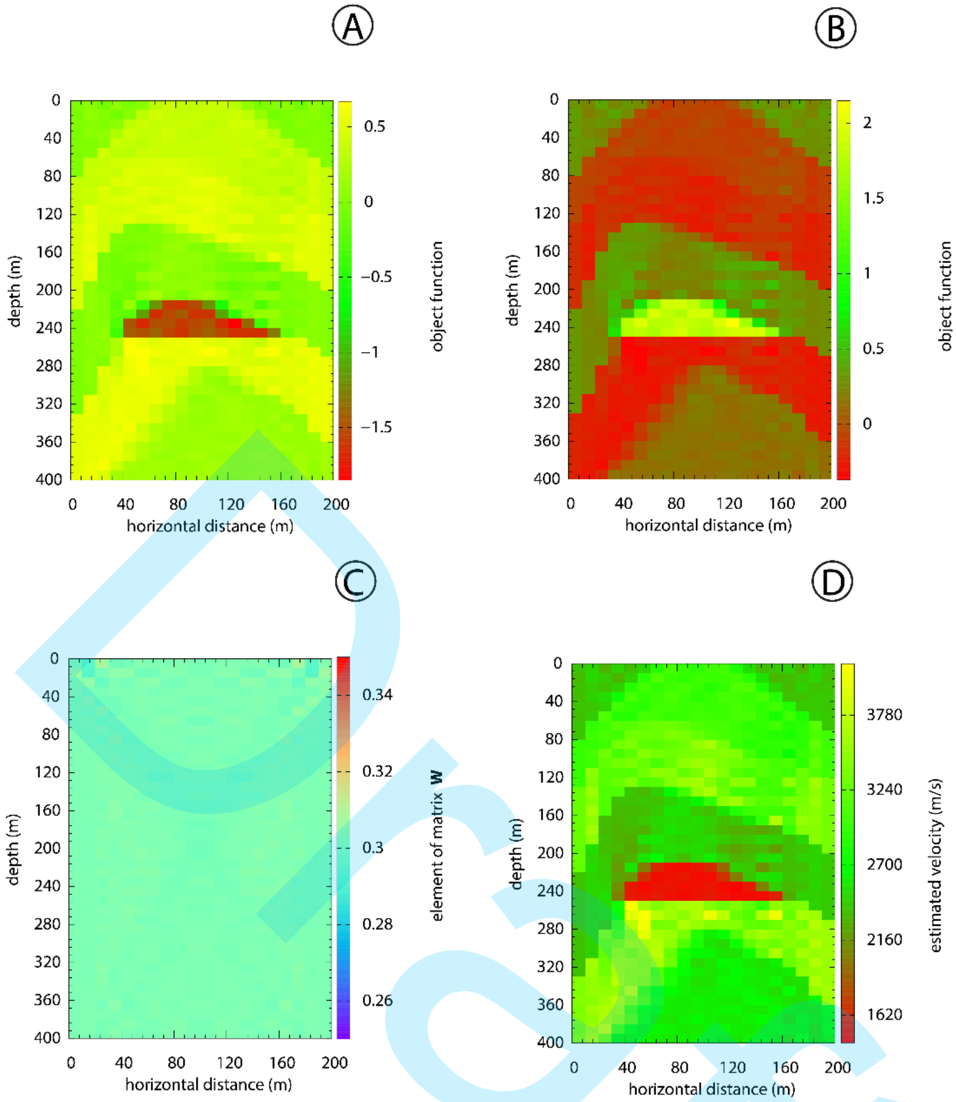

Figure 2: Model A, determined case, with noise-free data: (a) estimated model; (b) complementary estimated model; (c) pseudo-constant image; (d) estimated velocity model.

The addition of noise affects the results, as can be seen in Figure 3. Figure 3(a) shows the estimated object function with $\varepsilon_{noise} = 1\%$. Notice more fluctuation when compared to Figure 2(a). The same happens with estimated P-wave velocity, displayed in Figure 3(d). The letter quality of the solution, seen in Figures 3(a) and 3(d), is confirmed in Figure 3(c), far from having a constant velocity. Also, the values different from 0.3 in Figure 3(c) are more or less correspondent with a low recovery in Figure 3(a) or in Figure 3(d).

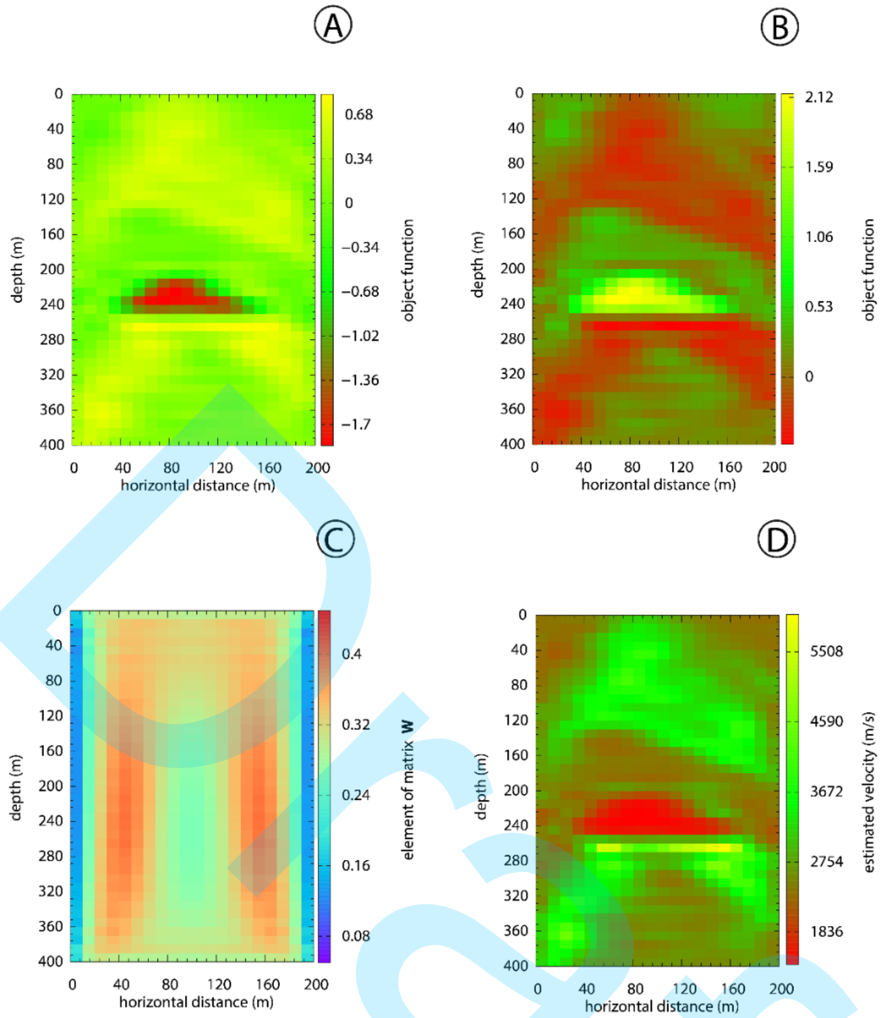

Figure 3: Model A, determined case, with noisy data: (a) estimated model; (b) complementary estimated model; (c) pseudo-constant image; (d) estimated velocity model.

For the overdetermined case, the estimated model and the complementary estimated model are shown, respectively, in Figures 4(a) and 4(b). Again, the sum of the images in Figures 4(a) and 4(b) shows a constant value, as can be seen in Figure 4(c). Similar to the determited case, the acoustic velocity, shown in Figure 4(d), shows a greater fluctuation than the object function, shown in Figure 4(a).

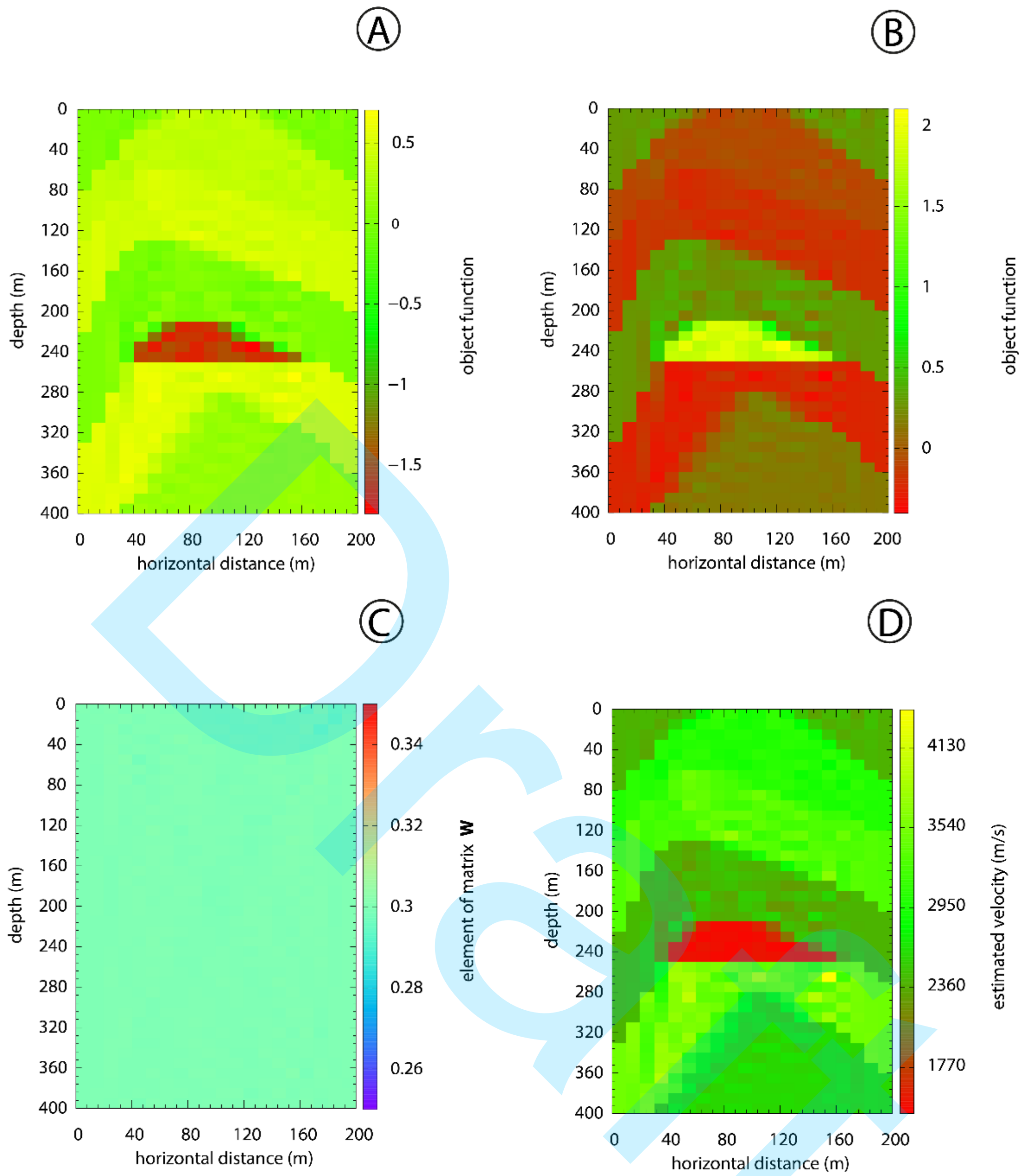

Figure 4: Model A, overdetermined case, with noise-free data: (a) estimated model; (b) complementary estimated model; (c) pseudo-constant image; (d) estimated velocity model.

Model B has 4000 square blocks, each with an edge of 50 meters. The whole model has 5000 meters in the horizontal direction and 2000 meters in depth. The vector $\mathbf{m}^{true}$ is shown in Figure 5(a). The acquisition geometry adopted in this model was surface seismics, with sources and receivers distributed along the surface. As with the previous model, all three configurations were used. The number of sources was kept constant, in this case 40 equally spaced sources. The underdetermined case had 25 receivers, which implies 1000 source-receiver pairs. The next case, the determined one, has 50 receivers, which now implies 2000 source-receiver pairs. Finally, the overdetermined case used 100 receivers, that is, 4000 source-receiver pairs. To employ Barbieri's criterion, the true matrix $\mathbf{W}$ is shown in Figure 5(b). Again, the value 0.3 was chosen for all elements of the matrix.

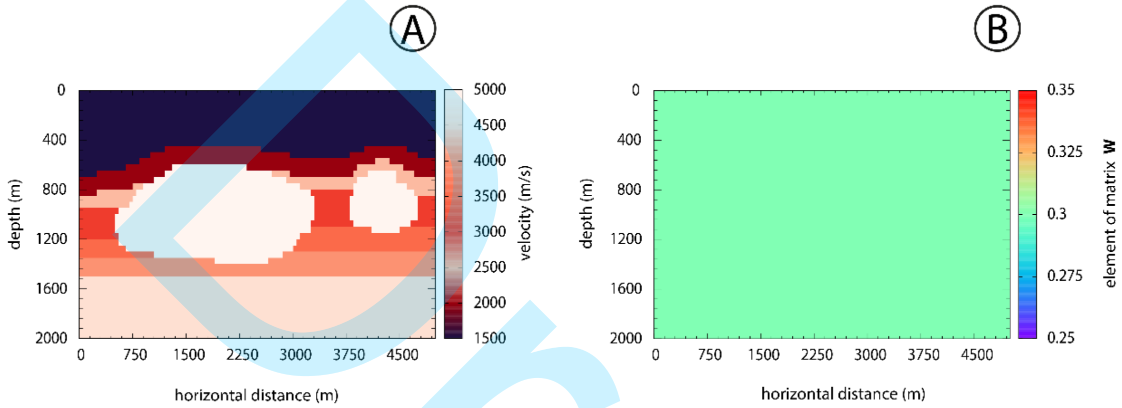

Figure 5: Model B. (a) True model with 4000 blocks, where the color bar indicates the P-wave velocities. (b) True matrix $\mathbf{W}$ with constant value of w_{ij} = 0.30 (dimensionless).

As in the previous model, the generalized inverse with regularization by matrices of second order derivatives was used. Again, in all simulations, the adopted working frequency was 50 Hz. Table 2 shows the results, for the simulation for noise-free data, as well as when the scattered field was contaminated with 1% and 5% RMS noise. The three data configurations (underdetermined, determined and overdetermined) were used.

Table 2: Inversion results of model B. The first three rows refer to the underdetermined case, the next three rows refer to the determinate case, and the last three rows present the results for the overdetermined case. The first column indicates the noise level. The second, third and fourth columns show the RMS deviations, respectively, between $\mathbf{d}^{obs}$ and $\mathbf{d}^{pre}$, $\mathbf{m}^{true}$ and $\mathbf{m}^{est}$, $\mathbf{w}$ and $\mathbf{w}^{est}$.

Noise (%)	ε_d (%)	ε_m (%)	ε_W (%)
0	≈ 0	37.14	3.98
1	≈ 0	76.24	745.09
5	0.24	78.50	745.09
0	≈ 0	12.14	2.97
1	4.55	89.13	86.42
5	10.19	85.10	5806.67
0	≈ 0	2.94	2.80
1	7.15	29.90	69.81
5	55.38	89.76	635.88

We present two results in figure form. The determined case is presented in Figure 6. Figures 6(a), 6(b) and 6(c) show, respectively, the estimated model, the complementary estimated model and the matrix $\mathbf{W}^{est}$. We can see in Figure 6(c) that the parts of the image where there is a deviation from the value of 0.3 correspond to the unresolved regions in the estimated model of Figure 6(a). The acoustic velocity is shown in Figure 6(d). In addition to the fact that Figure 6(d) shows a greater fluctuation than Figure 6(a), which also occurred in model A. The velocity values show a large fluctuation, although the shape of the main features has been well recovered, as well as the as the speeds of these features.

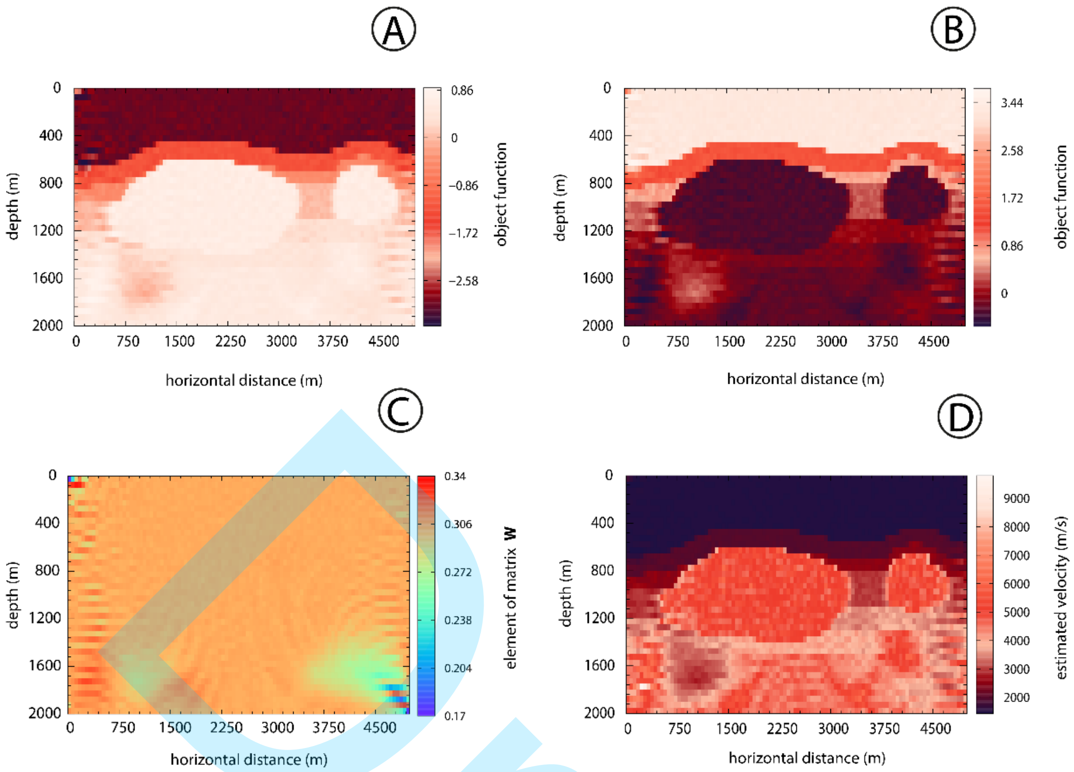

Figure 6: Model B, determined case, with noise-free data: (a) estimated model; (b) complementary estimated model; (c) pseudo-constant image; (d) estimated velocity model.

For the overdetermined case, the estimated model is shown in Figure 7(a) and the complementary estimated model in Figure 7(b). Compared to the result of the determined case, the resolution is much better. This is expected because of presence of more information. Again, the sum of the images in Figures 7(a) and 7(b), shown in Figure 7(c) does not present a constant value, and the few deviations from the value of 0.3 correspond in Figure 7(a) to the portions unresolved in Figure 7(a). The estimated P-wave velocities are shown in Figure 7(d), where we can observe a much smaller fluctuation than the determined case. In addition, the geological structures are well defined, and the estimated velocity values are very close to the true values.

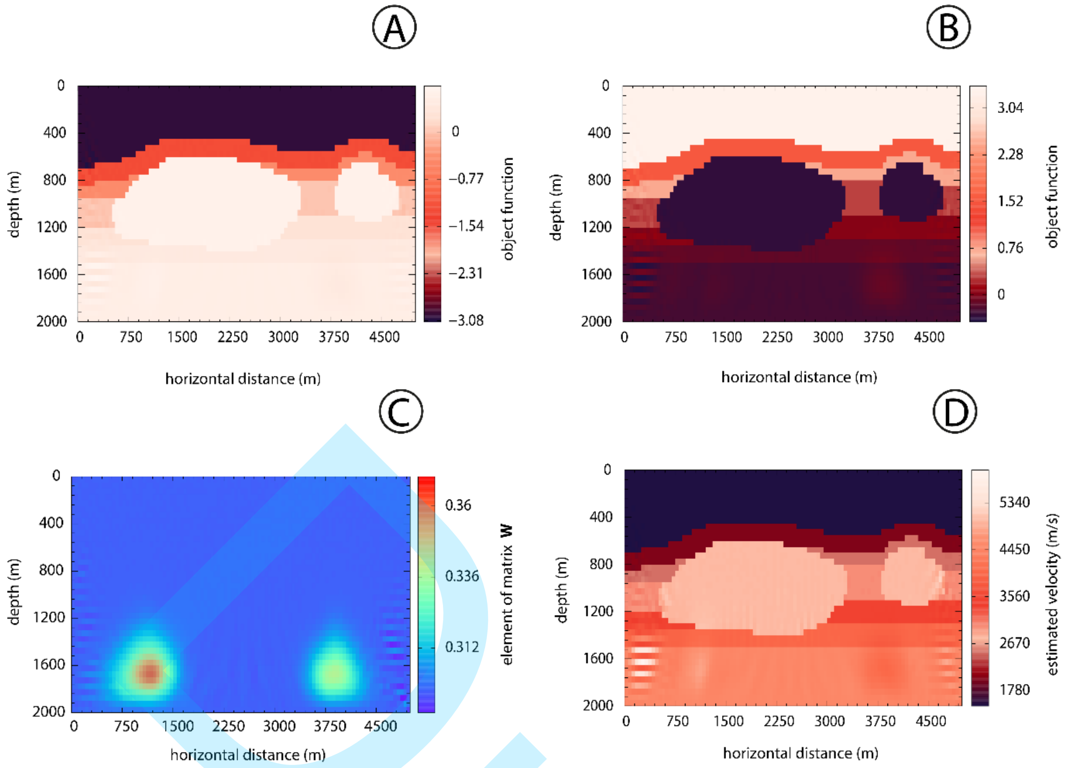

Figure 7: Model B, overdetermined case, with noise-free data: (a) estimated model; (b) complementary estimated model; (c) pseudo-constant image; (d) estimated velocity model.

CONCLUSIONS

Acoustic diffraction tomography is a frequency-domain inversion method used to estimate the P-wave velocities in the subsurface. And, because it is an ill-posed inverse problem, the application of a regularization procedure becomes essential. In this work we use regularization by derivative matrices. Very often, the solution of an inverse problem is not validated, especially in the case of real data. We consider two synthetic subsurface models, each with a specific data acquisition geometry, either well-to-well seismics or surface seismics. The so-called Barbieri criterion approach analyzes the sum of the estimated model with the complementary estimated model. This sum, represented by the matrix $\mathbf{W}^{est}$, is compared with a previously defined constant value $\mathbf{W}$. The similarity between the two matrices indicate a satisfactory estimated model, which was verified, for example, in the results of the first set of simulations. When the two matrices are visually different, as, for example, in the second set of simulations for the determined case, it can then be verified in which spatial portions of the estimated model, the inversion was not satisfactory. Finally, the deviation between $\mathbf{W}^{est}$ and $\mathbf{W}$ can be quantitatively evaluated, using an RMS estimator, which now allows comparing different results from the same set of simulations.

ACKNOWLEDGEMENTS

This work was carried out with the support of the Coordenação de Aperfeiçoamento de Pessoal de Nível Superior - Brasil (CAPES) – Financing Code 001. The authors also thank Fundação de Amparo à Pesquisa do Estado da Bahia (FAPESB) for project PIE00005/2016, Infrastructure Edict 003/2015. A. Bassrei thanks Conselho Nacional de Desenvolvimento Científico e Tecnológico (CNPq) for a research fellowship and for supporting the Instituto Nacional de Ciência e Tecnologia em Geofísica do Petróleo (INCT-GP) project.

REFERENCES

Barbieri, M., 1974, A criterion to evaluate three dimensional reconstructions from projections of unknown structures: Journal of Theoretical Biology, 48, 2, 451–467, doi: 10.1016/s0022-5193(74)80012-3.

Bassrei, A., 2000, Novel approaches for the solution and solution evaluation of linear and non-linear inverse problems in geophysics: Boletim da Sociedade Brasileira de Matemática Aplicada e Computacional, 2, 1–7.

Bejarano, S.L., and A. Bassrei, 2017, Critique of solutions in linearized inverse problems: Numerical experiments in traveltime tomography: Brazilian Journal of Geophysics, 34, 4, 495–508, doi: 10.22564/rbgf.v34i4.871.

Devaney, A., 1984, Geophysical diffraction tomography: IEEE Transactions on Geoscience and Remote Sensing, 1, 3–13, doi: 10.1109/TGRS.1984.350573.

Harris, J.M., 1987, Diffraction tomography with arrays of discrete sources and receivers: IEEE Transactions on Geoscience and Remote Sensing, GE-25, 448–455, doi: 10.1109/TGRS.1987.289856.

Lo, T.-W., and P.L. Inderwiesen, 1994, Fundamentals of Seismic Tomography: Society of Exploration Geophysicists: Tulsa, OK, 187 pp, doi:

10.1190/1.9781560802334.

Menke, W., 2018, Geophysical Data Analysis: Discrete Inverse Theory: 4th ed., Academic Press: San Diego, US. 330 pp, doi: 10.1016/C2016-0-05203-8.

Penrose, R., 1955, A generalized inverse for matrices: Mathematical Proceedings of the Cambridge Philosophical Society, 51, 3, 406–413, doi: 10.1017/S0305004100030401.

Sande, D., A. Bassrei, and J. Harris, 2019, New iterative and multi-frequency approaches in geophysical diffraction tomography: Brazilian Journal of Geophysics, 37, 187–197, doi: 10.22564/rbgf.v37i2.2000.

Santos, E.T.F., and A. Bassrei, 2007, L- and θ-curve approaches for the selection of regularization parameter in geophysical diffraction tomography: Computers & Geosciences, 33, 618–629, doi: 10.1016/j.cageo.2006.08.013.

Santos, E.T.F., J.M. Harris, A. Bassrei, and J.C. Costa, 2009, Trigonal meshes in diffraction tomography with optimum regularization: an application for carbon sequestration monitoring: Journal of Seismic Exploration, 18, 135–156.

Santos, E.T.F., A. Bassrei, and J.M. Harris, 2021, The generalized cross validation method for the selection of regularization parameter in geophysical diffraction tomography: Brazilian Journal of Geophysics, 39, 1, 71–83, doi: 10.22564/rbgf.v38i3.2061.

Silva, C.J.M.G., and A. Bassrei, 2016, Singular value selection and generalized cross validation in multi-frequency seismic diffraction tomography for CO_2 injection monitoring: Brazilian Journal of Geophysics, 34, 175–192, doi: 10.22564/rbgf.v34i2.791.

Twomey, S., 1963, On the numerical solution of Fredholm integral equations of the first kind by the inversion of the linear system produced by quadrature: Journal of the Association of Computing Machines, 10, 97–101, doi: 10.1145/321150.321157.

Wu, R.-S., and M.N. Toksöz, 1987, Diffraction tomography and multisource holography applied to seismic imaging: Geophysics, 52, 11–25, doi: 10.1190/1.1442237.

Mascarenhas, D.W.S.: performed the data simulation, generated the figures and tables, and wrote the first version of the manuscript; **Bassrei, A.:** sugested and supervised the research, contributed to the results discussion, reviewed and translated the manuscript.